Diluting a triangular-lattice spin liquid: Synthesis and characterization of NaYb$_{1-x}$Lu$_x$S$_2$ single crystals

Ellen Häußler [1], Jörg Sichelschmidt [2], Michael Baenitz [2], Eric C. Andrade [3], Matthias Vojta,[4] and Thomas Doert [1,*]

[1]*Fakultät für Chemie und Lebensmittelchemie, Technische Universität Dresden, 01062 Dresden, Germany*

[2]*Max Planck Institute for Chemical Physics of Solids (MPI-CPfS), 01187 Dresden, Germany*

[3]*Instituto de Física de São Carlos, Universidade de São Paulo, C.P. 369, São Carlos, São Paulo 13560-970, Brazil*

[4]*Institut für Theoretische Physik and Würzburg-Dresden Cluster of Excellence ct.qmat, Technische Universität Dresden, 01062 Dresden, Germany*

Yb-based magnets, with a perfect triangular lattice of pseudospin-$\frac{1}{2}$ Yb^{3+} ions, have emerged as candidates for realizing a quantum spin-liquid state, with NaYbS$_2$ being a prominent example. Here, we present the solid-solution series NaYb$_{1-x}$Lu$_x$S$_2$ with well-defined single crystals over the entire substitution range $0 \leqslant x \leqslant 1$. Chemical and structural analysis indicate a statistically homogeneous replacement of Yb^{3+} by Lu^{3+} ions. We magnetically characterize the relatively small single crystals using electron spin resonance (ESR). Below 30 K, the ESR intensity can be well described by a Curie-Weiss function for all x, with a decreasing Weiss temperature with increasing Lu content. This reduction of the average magnetic interaction upon Lu substitution is also supported by magnetization measurements. Importantly, no signs of magnetic or spin-glass order are detected down to 2 K for any x. For $x > 0.5$, the ESR linewidth strongly increases, indicating the breakup of the magnetic system into disconnected clusters, as expected from percolation physics. The experimental magnetization data are found to be in good agreement for all x with results of classical Monte Carlo simulations for a triangular-lattice Heisenberg model, amended with a small second-neighbor interaction. Taken together, our results establish NaYb$_{1-x}$Lu$_x$S$_2$ as a family of diluted triangular-lattice spin liquids.

I. INTRODUCTION

Although the existence of quantum spin liquid (QSL) states was proposed by Anderson [1] nearly 50 years ago, the number of comprehensively studied candidate materials has increased only recently [2]. A number of promising materials only qualify as proximate QSLs, such as α-RuCl$_3$ [3] and Na$_2$IrO$_3$ [4], exhibiting long-range magnetic order at low temperatures. Others are debated because of considerable atomic disorder, such as YbMgGaO$_4$ [5,6] and H$_3$LiIr$_2$O$_6$ [7], raising doubts on the intrinsic nature of the observed spin-liquid features.

In the quest for new spin-liquid compounds, ABX_2 compounds with α-NaFeO$_2$ structures (with A being a nonmagnetic monovalent cation, B a magnetic trivalent cation, and X a divalent anion) have attracted considerable attention since NaYbS$_2$ with Yb^{3+} ions on a perfect triangular lattice was proposed as a putative QSL material [8,9], Fig. 1. Further Yb-based compounds such as NaYbO$_2$ [10,11] and NaYbSe$_2$ [12] were investigated soon afterwards and also found to display no magnetic order down to 50 mK. Triangular lattice Yb compounds have thus established themselves as an important class of spin-orbit-entangled spin liquids [13]. Note that the structure type of these compounds is frequently referred to as delafossite, although the mineral delafossite CuFeO$_2$ features

A cations in linear coordination [14]. In NaREX_2 and related compounds, A and B cations are both found in octahedral coordination. This atomic arrangement should be referred to as α-NaFeO$_2$ type. α-NaFeO$_2$ and CuFeO$_2$ are isopointal; they adopt the same space group type $R\bar{3}m$ with similar lattice parameters, and respective atoms occupy the same Wyckoff sites, but they are not isotypic in a strict sense. Indeed, ABX_2 compounds with α-NaFeO$_2$-type crystal structure provide a perfect geometrical basis for the realization of a QSL state, as different magnetic ions with predominant antiferromagnetic interactions can be placed on the B sites forming a regular triangular lattice. Atomic site disorder does not seem to play a dominant role; at least no evidence was found in single-crystal diffraction, nuclear magnetic resonance, or electron spin resonance (ESR) data of NaYbS$_2$ or NaYbSe$_2$, e.g., Refs. [8,10,12,15]. The layers of magnetically active B ions are separated by nonmagnetic AX_6 octahedral layers, which give the structure a quasi-two-dimensional character with respect to magnetism (Fig. 1).

Theoretically, triangular-lattice spin models with either Heisenberg or spin-anisotropic exchange interactions have been shown to display QSL phases, accompanied by fractionalization and deconfinement, in certain ranges of their parameter space [16–21]. However, precise model parameters to describe the magnetism of such Yb compounds are not known to date. With a clean candidate QSL material at hand, studying its behavior under chemical substitution defines a highly interesting field of research. This includes the
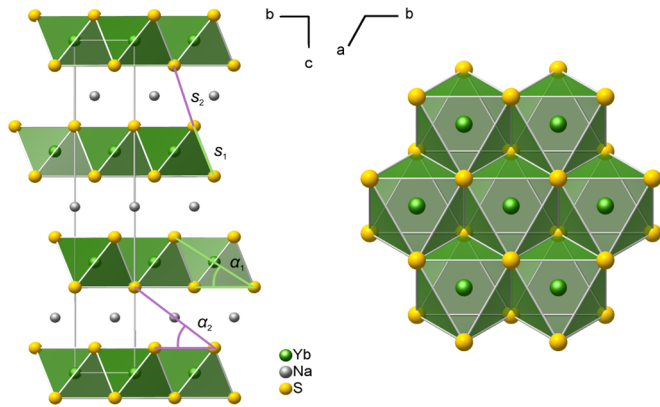
---

*thomas.doert@tu-dresden.de

FIG. 1. Crystal structure of NaYbS$_2$ in $R\bar{3}m$ viewed along a (left) and section of an YbS$_6$ layer (right). The unit cell is depicted in light gray. Interlayer sulfur-sulfur distances s_1 (light green) and s_2 (lavender) as well as the torsion angles α_1 (light green) and α_2 (lavender) of the YbS$_6$ and NaS$_6$ octahedra, respectively, are highlighted; see text for details.

physics of carrier doping to achieve metallic or superconducting states [1,22,23], magnetic dilution [24], and various forms of bond disorder [25–27]. Magnetic dilution, achieved by replacing magnetic with nonmagnetic ions, is particularly interesting, as the introduction of magnetic vacancies into quantum paramagnets can distinguish confined from deconfined phases [28]; here, *(de)confined* refers to the properties of the gauge field in a description in terms of fractionalized particles coupled to an emergent gauge field. In confined (i.e., conventional nonfractionalized) phases, vacancies introduce quantized magnetic moments which generically lead to magnetic [24] (or spin-glass [29]) order at low temperatures. A nice example is the quantum-dimer magnet TlCuCl$_3$ once small amounts of Cu are replaced by Mg [30]. In contrast, in deconfined (i.e., fractionalized) phases, no vacancy-induced moments are expected [28,31], such that spin-liquid behavior survives dilution (although special counterexamples have been discussed theoretically [32]). A number of theoretical studies have characterized spin liquids according to their response to the introduction of vacancies [31,33,34]. However, in-depth experimental studies on high-quality single crystals of corresponding dilution series of QSL candidates are rare.

Parenthetically, we note that bond disorder has been argued to induce spin-liquid-like behavior in magnets which display long-range order in the clean limit [35–38]. Moreover, strong dilution has been found to determine the magnetic state of the triangular-lattice system Y$_2$CuTiO$_6$ [39].

It is the purpose of this paper to study magnetic dilution for a Yb spin liquid on a triangular lattice. We investigate how the local and global magnetic properties evolve in the solid-solution series NaYb$_{1-x}$Lu$_x$S$_2$ with $0 \leqslant x \leqslant 1$ for which we can prepare single crystals covering the whole range of x. With increasing substitution of Yb^{3+} by nonmagnetic Lu^{3+}, we expect the network of exchange couplings to be weakened, such that the $x = 0$ QSL eventually evolves into a state with single-ion paramagnetic properties as $x \to 1$. We characterize the evolution and interplay of magnetic interactions in the substitution series NaYb$_{1-x}$Lu$_x$S$_2$ by ESR and magnetic

susceptibility measurements. Indeed, ESR is the method of choice for small single crystals [40]. For example, the nature of the ground state of a spin-liquid candidate in the organic salts could be successfully elucidated [41]. NaYbS$_2$ has proven to be ideally suited for investigating the spin dynamics of Yb^{3+} by ESR [42]: a well-resolved and narrow Yb^{3+} spin resonance allowed an accurate characterization of the g-factor anisotropy and the static and dynamic properties of the Yb^{3+} magnetic susceptibility.

Our experimental data are consistent with spin-liquid-like behavior of NaYb$_{1-x}$Lu$_x$S$_2$ in a wide composition range. We do not detect signs of magnetic order down to 2 K for all x. For $x > 0.5$, we observe a strong increase in the ESR linewidth, indicating a breakup of the magnetic system into percolation clusters and suggesting that exchange interactions beyond nearest neighbors are small. Our measured temperature-dependent susceptibilities are in agreement with corresponding data from classical Monte Carlo (MC) simulations of a J_1-J_2 Heisenberg model with random dilution. Together, these results confirm that our crystals display a statistical distribution of Lu dopants and represent a family of diluted triangular-lattice QSLs.

II. EXPERIMENTAL

All samples of the solid-solution series NaYb$_{1-x}$Lu$_x$S$_2$ were prepared by a slightly modified procedure adopted from Masuda *et al.* [43] starting from dried Na$_2$S (see Supplemental Material [44] for its preparation), Yb$_2$O$_3$ (Heraeus, 99.9%), Lu$_2$O$_3$ (ChemPUR, 99.99%), and CS$_2$ (Honeywell, Riedel-de Haën, 99.9%) at 1050 °C in a protective argon atmosphere, following the idealized reaction equation:

$$2\,\mathrm{Na_2S} + 2\,RE_2\mathrm{O_3} + 3\,\mathrm{CS_2} \to 4\,\mathrm{Na}RE\mathrm{S_2} + 3\,\mathrm{CO_2}. \quad (1)$$
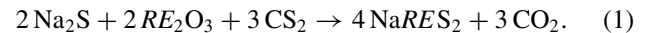
Na$_2$S (2500 mg, 32 mmol, and 29 equivalents) and the respective amounts of Yb$_2$O$_3$ ($1 - x$ eqs.) and Lu$_2$O$_3$ (x eqs.) were mixed in the molar ratios and filled in a glassy carbon boat which was placed in a ceramic tube inside a tubular furnace (Fig. S1 in the Supplemental Material [44]). The large excess of Na$_2$S used in the reaction serves as flux material to foster crystal growth. The apparatus including a 1 L flask as a CS$_2$ reservoir was flushed with argon for 30 min before the furnace temperature was raised to 1050 °C within 3 h under an unloaded stream of argon ($\sim$2 L/h). While dwelling for 1 h, CS$_2$ was transported to the reaction zone by bubbling argon ($\sim$5 L/h) through the reservoir.

Afterwards, the apparatus was cooled down under a stream of unloaded argon ($\sim$2 L/h) to 600 °C within 6 h before the furnace was switched off. Throughout the whole procedure, $\sim$20 mL ($\sim$330 mmol) of CS$_2$ were consumed.

The reaction product was leached with water to remove the flux material, and the target compound was filtered-off and washed with water and ethanol. Leftovers of small black particles, presumably carbon, were decanted after ultrasonication in ethanol. After vacuum drying, the remaining product was found to consist of transparent, yellow hexagonal platelets with diameters ranging from $\sim$10 to 800 μm. Crystal surfaces show faint tarnishing after exposure to moist air for several days or weeks. Crystals used for ESR and magnetization measurements were stored under inert conditions, thus.

Phase purity and the evolution of the lattice parameters were evaluated by x-ray powder diffraction (PXRD). For these measurements, the samples were mixed with a Si standard and filled in glass capillaries. Rietveld refinements were done with TOPAS Academic [45] in the range of 14° to 130° 2θ, using the atomic positions of NaYbS$_2$ [46] as a starting model. Single-crystal diffraction data of selected crystals were collected to confirm the Rietveld results [47,48].

Elemental ratios were measured on several embedded and polished crystals via electron dispersive spectroscopy (EDX) in combination with imaging respective samples with a scanning electron microscope (SEM). The chemical composition of selected samples was additionally checked by optical emission spectroscopy (ICP-OES) and combustion analysis. Optical bandgaps were determined from diffuse reflection spectra using a Varian Cary 400 UV/Vis spectrometer [49,50]. Magnetization measurements were performed with a Quantum Design superconducting quantum interference device vibrating sample magnetometer. Crystals used for the magnetization measurements were taken from the same batches as those for the ESR experiments. ESR experiments were performed at X-band frequencies ($\nu = 9.4$ GHz) using a continuous-wave ESR spectrometer. The ESR experiments were performed on single-crystalline platelets with a typical size of $0.4 \times 0.4 \times 0.05$ mm^3. The sample temperature was set with a helium-flow cryostat allowing for temperatures between 2.7 and 300 K [51].

Further details on experimental methods are stated in the Supplemental Material [44].

III. RESULTS AND DISCUSSION

A. Crystal growth, optical and chemical properties

NaYb$_{1-x}$Lu$_x$S$_2$ crystals grow as hexagonal platelets or antiprisms with an aspect ratio of (10–20) : 1. The typical morphology of the crystals can be seen in the images in Fig. 2 taken with a light microscope and a SEM, respectively. Over the major part of the substitution range, the crystals remain bright yellow, like the ternary border compound NaYbS$_2$. Crystals with high lutetium content ($x > 0.8$) are pale yellow.

The bandgaps of NaYbS$_2$ and NaLuS$_2$ were determined to be 2.74 and 3.94 eV, matching the reported data of 2.7 eV [9] and 4.08 eV [52], respectively. The bandgaps of NaYb$_{1-x}$Lu$_x$S$_2$ remain constant at $\sim$2.73 eV until $x \leqslant 0.8$, but jump to 3.87 eV for $x = 0.9$ (Fig. S2 in the Supplemental Material [44]). According to band structure calculations of isostructural rare-earth-metal-based compounds, the bandgap
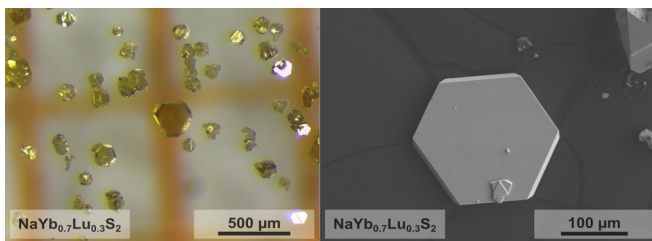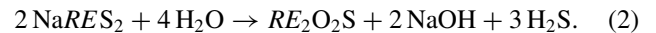
mainly results from the distance between the occupied chalcogenide p-states and the RE d-state-dominated conduction band [53]. The sudden step in the evolution of the bandgaps and the corresponding color change cannot be explained by the observed smooth change of the lattice parameters, see below. The UV/Vis spectrum of NaLuS$_2$ shows only one absorption edge at 315 nm, whereas the spectrum of NaYbS$_2$ exhibits an additional broad band at 360 nm (see Fig. S3 in the Supplemental Material [44]). The latter is attributed to a sulfur-to-RE charge transfer (CT) transition [54] and can be observed in all compounds with $x \leqslant 0.8$. As the low-energy slope of this CT transition is now used to determine the absorption edge, a considerable drop in bandgaps is computed in accordance with the colors of the samples.

Upon grinding of the crystals under ambient conditions, a faint H$_2$S odor was recognized. X-ray powder diffractograms of ground samples showed small reflections of the respective oxysulfides RE_2O$_2$S, so that we assume the following slow decomposition of the ground sample fostered by humidity from air and/or adsorbed water:

$$2\,\mathrm{Na}RE\mathrm{S}_2 + 4\,\mathrm{H}_2\mathrm{O} \rightarrow RE_2\mathrm{O}_2\mathrm{S} + 2\,\mathrm{NaOH} + 3\,\mathrm{H}_2\mathrm{S}. \quad (2)$$

Reflections of NaOH were not observed in PXRD of the ground samples, probably due to the formation of non-crystalline hydrates of NaOH and/or Na$_2$S. Traces of the oxysulfide were only found after grinding, i.e., in samples with small particles and large surfaces. Crystals stored under inert conditions are stable for years.

B. Chemical and structural characterization

Chemical analyses confirm the composition of the samples within the error of the respective method, Table SI in the Supplemental Material [44]. The EDX-based sulfur contents of the crystals [47(1) at. %] was always found slightly below the bulk value from ICP-OES and combustion analysis [49.1(8) at. %]; we attribute this to the embedding and wet-chemical polishing procedure applied before EDX. Carbon (<1 at. %) and oxygen amounts (<0.6 at. %) of the bulk polycrystalline samples were generally considered as insignificant for the ESR and magnetic measurements, which were all performed on selected single crystals.

No peak splitting or additional reflections were found in the x-ray powder diagrams of the samples. Instead, all reflections can be indexed with space group $R\bar{3}m$ and unit cell dimensions close to the border phases NaYbS$_2$ and NaLuS$_2$ so that a complete substitution series NaYb$_{1-x}$Lu$_x$S$_2$ ($0 \leqslant x \leqslant 1$) without phase separation or symmetry reduction can be assumed. The PXRDs of all samples exhibit a strong preferred orientation along the [001] direction. The lattice parameters were refined in the course of the Rietveld fits using the fundamental parameter approach and a manually modeled background to take care of the enhanced background at low angles (between 14° and 30° 2θ) caused by the glass capillary.

The refined lattice parameters are stated in Table SII in the Supplemental Material [44] and graphically depicted in Fig. 3 against the amount of lutetium. For both ternary boundary phases NaYbS$_2$ ($x = 0$) and NaLuS$_2$ ($x = 1$), literature structure data were confirmed. The atomic positions of NaYbS$_2$ were used as a start model for the Rietveld refinements,

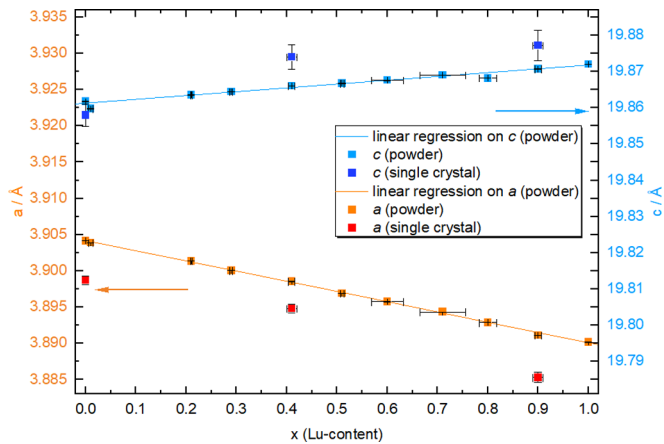FIG. 2. Images of crystals taken under an optical microscope (left panel) and by scanning electron microscopy (right panel).

FIG. 3. Refined lattice parameters a and c of $NaYb_{1-x}Lu_xS_2$ samples derived from powder and single-crystal data.

FIG. 4. Left frame: Typical X-band ESR spectra at $T = 20$ K of Yb^{3+} for selected x in $NaYb_{1-x}Lu_xS_2$ single crystals and for indicated field orientations. Solid lines indicate single Lorentzian line shapes. Upper right frame: ESR g-factor dependence for $x = 0.5$, depending on the field orientation with respect to the crystalline c axis. Lower right frame: Yb amount dependence of the g-factor anisotropy for $T = 20$ K.

considering a mixed occupancy of the Wyckoff site $2a$ with Yb and Lu for all compounds with $0 < x < 1$. As the electron counts of the two rare-earth elements differ by only one, a free refinement of the occupation parameters is merely possible. Instead, the site occupancy factors for both elements were taken from the analytical data (EDX, ICP-OES) and kept fixed during the refinements. We found neither evidence for other mixed occupied sites or site defects nor indications for an ordered superstructure at any degree of substitution from these fits. The result of the Rietveld refinement for $NaYb_{0.71}Lu_{0.21}S_2$ is depicted as one example in Fig. S4 in the Supplemental Material [44].

No peak spitting was observed in the diffraction images of selected single crystals of $NaYb_{1-x}Lu_xS_2$ (with $x = 0$, 0.4, and 0.9) samples either, confirming the PXRD-based Rietveld results. The respective structure models could be refined to good agreement values in space group $R\bar{3}m$; no additional peak positions, suspicious displacement parameters, or residual electron density maxima were found. The refinement of the Na and *RE* site occupancy factors did not deviate from unity within standard deviations, i.e., there is no evidence for Na/*RE* site disorder from single-crystal diffraction data. Figure 1 depicts the crystal structure of $NaYbS_2$ as an example. Crystallographic data and refinement parameters are compiled in Tables SIII, SIV, and SV in the Supplemental Material [44].

As can be seen from Fig. 3, the lattice parameter a decreases linearly with increasing Lu content. This can be easily understood as the larger Yb^{3+} ion ($r = 1.008$ Å) is progressively replaced by the smaller Lu^{3+} ion ($r = 1.001$ Å; both radii are given for coordination number 6 [55]). The c lattice parameter, however, gets elongated with increasing Lu content. Note that the change of the lattice parameter c is about seven times smaller than the change in a (0.05% for c, 0.35% for a), so that the unit cell volume decreases slightly (Fig. S5 in the Supplemental Material [44]). The slight deviations between powder and single-crystal data can be attributed to the use of different devices and wavelengths.

Upon substitution, not only the lattice in the ab plane is compressed, but also the YbS_6 octahedra show a similar trend, as can be seen from the decreasing interlayer sulfur-
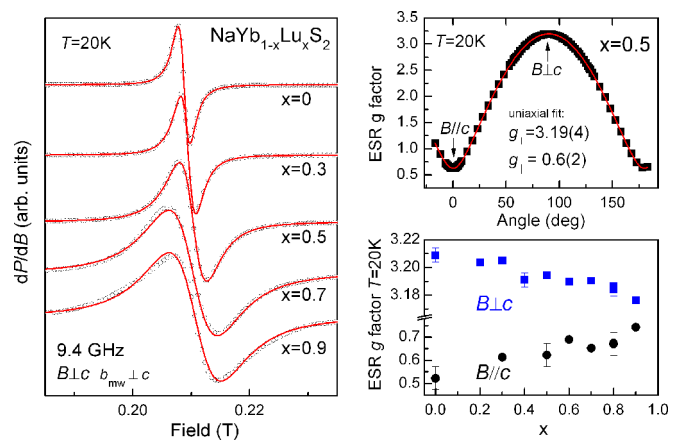
sulfur distances s_1 and the torsion angle α_1 of YbS_6 octahedra (Fig. 1). Unfortunately, the powder-based structure data show some scattering, although displacement parameters and site occupation factor were kept fixed to reduce correlations in the Rietveld refinements. The single-crystal data, however, indicate the same trend. The overall changes of 0.6% for s_1 and 0.2% for α_1 are in the same range as those of the lattice parameter a. Consistent with the slight increase in lattice parameter c, the NaS_6 octahedra slightly increase as well, which can be concluded from the sulfur-sulfur interlayer distances s_2 and the torsion angle α_2. The changes of the interatomic distances and torsion angles are depicted in Figs. S6 and S7 in the Supplemental Material [44].

C. ESR spectroscopy

Typical ESR spectra are shown in Fig. 4, left frame. The deviations from an ideal Lorentzian shape are small but visible. For samples with $x \geqslant 0.8$, a multiple-line structure appears which is consistent with a Yb-hyperfine split resonance. As shown in Fig. S8 in the Supplemental Material [44], this hyperfine split structure is most pronounced for $x = 0.9$, which indicates a very weak interaction among the Yb spins for this concentration [56,57]. Delafossite-related Yb compounds show strong anisotropies of their Yb^{3+} resonance field [58] caused by uniaxial g value anisotropies. For $NaYb_{1-x}Lu_xS_2$, this anisotropy is retained for all investigated Yb contents and is exemplarily shown for $x = 0.5$ in Fig. 4 (upper right frame). A clear x dependence of the anisotropy $g_\perp/g_\parallel$ can be resolved, as shown in the lower right frame of Fig. 4.

The ESR linewidth behavior $\Delta B(T)$ is shown in Fig. 5. Toward high temperatures, as seen in related Yb compounds [58], $\Delta B(T)$ shows the same exponential increase, being characteristic for an Orbach-type spin lattice relaxation $\Delta B \propto 1/[\exp(\Delta/T) - 1]$ (red solid lines). This relaxation involves the first crystalline-electric field (CEF) split electronic energy level Δ above the ground state [59]. We obtained
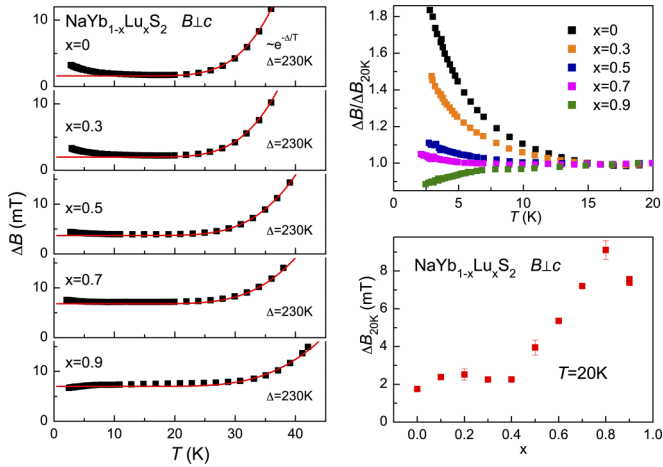
FIG. 5. Temperature and x dependence of the ESR linewidth ΔB of $NaYb_{1-x}Lu_xS_2$ single crystals. Left frame: Toward higher temperatures, the solid lines indicate a relaxation via the first excited crystalline-electric field (CEF) level of Yb^{3+} at ΔK. Right upper frame: Low-temperature behavior of ΔB normalized by its value at $T = 20$ K. Right lower frame: x dependence of the linewidth at $T = 20$ K.

$\Delta = 230 \pm 50$ K, independent of x, indicating that mainly properties of the CEF ground state are affected by changes of the Yb^{3+} amount, i.e., changes in the CEF distortion. Noteworthy, changes of the ground-state properties are well resolved in changes of the g-factor anisotropy, see Fig. 4.

Toward low temperatures, as illustrated by a normalized $\Delta B(T)$ representation, Fig. 5 right upper frame, the linewidth behavior clearly depends on the Yb^{3+} amount (see also the nonnormalized plot Fig. S9 in the Supplemental Material [44]). For $x < 0.8$, the linewidths display a moderate broadening, indicating the increasing influence of intersite spin correlations [58]. For $x \geqslant 0.8$, $\Delta B(T)$ shows, instead of an increase, a decrease becoming pronounced below $T \approx 10$ K. Such temperature dependence is unveiled by a diminished spin-spin correlation, as it appears concomitant to a single-ion typical hyperfine structure in the line shape. It indicates a direct relaxation of spin-orbit coupled spins to lattice vibrations through a modulation of the ligand field, which leads to a linear temperature dependence if a direct phonon process dominates, for instance [59,60].

The linewidth also clearly depends on the Yb content, as illustrated for $T = 20$ K in the right lower frame of Fig. 5. With decreasing Yb content ΔB first stays at values ~ 2 mT for $x < 0.5$ before rising up to $\Delta B = 7.5$ mT for $x = 0.9$. This indicates, for $x > 0.5$, an additional broadening arising from an inhomogeneous Yb distribution, as found for disconnected magnetic clusters, for instance. Note that, at the same time, the abovementioned contribution of intersite spin correlations is strongly reduced but still visible up to $x \leqslant 0.8$ in the line broadening toward low temperatures.

The ESR intensity $I_{ESR} \equiv \chi_{ESR}$ is a direct measure of the spin-probe magnetic susceptibility along the direction of the microwave magnetic field b_{mw} [61]. As shown in Fig. 6, below ~ 30 K, χ_{ESR} is consistent with a Curie-Weiss (CW) law $\propto (T - \theta)^{-1}$ with negative Weiss temperatures θ. A decreasing
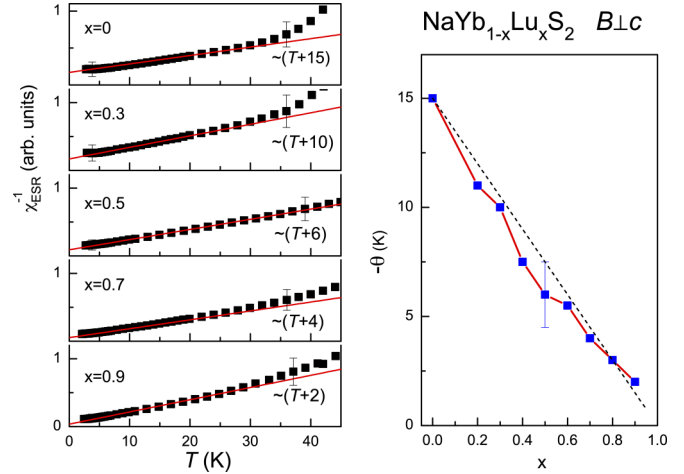

FIG. 6. Temperature dependence of the reciprocal ESR intensity χ_{ESR}^{-1} for various x in $NaYb_{1-x}Lu_xS_2$ single crystals with their c axes aligned perpendicular to the external field B and the microwave field b_{mw}. Solid lines indicate low-temperature linear behavior $\propto (T - \theta)$ with Weiss temperatures θ as plotted in the right frame. Dashed line corresponds to $(1 - x)15$ K.

Yb^{3+} content leads to a continuously decreasing $-\theta$ (right frame in Fig. 6), as expected for decreasing antiferromagnetic correlations among the Yb^{3+} spins. This behavior agrees well with measurements of the bulk magnetic susceptibility, as illustrated for $x = 0, 0.5$, and 0.8 in Fig. 7. Note, however, that the Weiss temperatures obtained from bulk susceptibility and ESR intensity do not exactly match. The reason for this difference, being also observed in other compounds [13,61–63], could be that spin correlations are probed by ESR locally at the Yb sites in contrast to magnetic susceptibility which is a nonlocal and nondynamical probe.
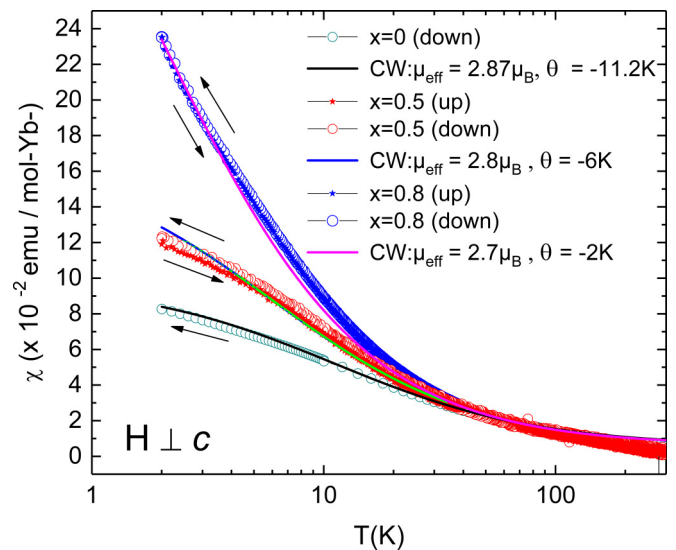

FIG. 7. Magnetic susceptibility for $NaYb_{1-x}Lu_xS_2$ crystals with $x = 0, 0.5$, and 0.8 for fields applied perpendicular to the crystallographic c direction. The solid lines represent a Curie-Weiss (CW) fit to the data below 80 K. Measurements for $x = 0.5$ and 0.8 are performed in zero-field-cooled (zfc; up)/field-cooled (fc; down) mode.

D. Susceptibility

Figure 7 shows the temperature dependence of the magnetic susceptibility of NaYb$_{1-x}$Lu$_x$S$_2$ crystals with $x = 0, 0.5,$ and 0.8 studied at the ESR magnetic field of ~ 0.21 T for fields applied perpendicular to the crystallographic c direction. Below 80 K, the data can be well described by a CW curve. The CW fits show that the Weiss temperature decreases sharply with increasing Lu amount, while the effective moment at Yb hardly changes. These results are in a good agreement with the ESR measurements, i.e., a strong change in the Weiss temperature is observed, while the g factor decreases only moderately. The zero-field-cooled (zfc) and field-cooled (fc) mode measurements do not show any branching or pronounced hysteretic behavior. We take this as evidence for the absence of magnetic domains, structural clusters, or glassy effects. As shown for the example of NaYb$_{1-x}$Lu$_x$S$_2$ with $x = 0.8$, only a small difference of the order of ~ 0.01 T is visible in the magnetization curve (at 10 K) with ascending and descending magnetic field (Figs. S10 and S11 in the Supplemental Material [44]).

E. MC simulations

A minimal model to capture the physics of the delafossite-like spin-liquid candidate compounds is the J_1-J_2 Heisenberg model on the triangular lattice:

$$\mathcal{H} = J_1 \sum_{\langle ij \rangle} \vec{S}_i \cdot \vec{S}_j + J_2 \sum_{\langle\langle ij \rangle\rangle} \vec{S}_i \cdot \vec{S}_j \qquad (3)$$

with antiferromagnetic first-neighbor and second-neighbor couplings J_1 and J_2, respectively. The classical ground state of this model depends on the ratio J_2/J_1: For $J_2/J_1 < \frac{1}{8}$, a coplanar 120° state is realized, while $J_2/J_1 > \frac{1}{8}$ yields a collinear four-sublattice state [64]. For quantum spins $S = \frac{1}{2}$, numerics indicate the existence of a fractionalized QSL for $0.08 < J_2/J_1 < 0.16$ whose precise nature, however, has not been clarified beyond doubt [16–19]. With spin anisotropies included, the nearest-neighbor exchange model has also been shown to host QSL phases [20,21]. At this point, there is no definite consensus on the microscopic model faithfully describing the triangular spin-liquid candidates.

To theoretically assess the effect of dilution on the magnetic properties of NaYbS$_2$ at elevated temperatures, we confine ourselves to a study of Eq. (3) in the classical limit. We perform classical MC simulations on lattices of linear size L and periodic boundary conditions. Our spins are then replaced by classical vectors of fixed length S. Depletion is simulated by randomly removing a fraction x of spins, with the total number of spins $N_s = (1 - x)N$. We perform equilibrium MC simulations using single-site updates with a combination of the heat-bath and microcanonical (or overrelaxation) methods. For simulations at high temperatures, the simulations reach equilibrium quickly, and tens of thousands of MC steps per spin are sufficient to evaluate the thermal averages. Disorder averages are taken over N_{rl} samples, with $N_{rl} \sim 100$.

Before discussing numerical results, we recall that previous work on vacancies in noncollinear triangular-lattice antiferromagnets has shown that an isolated vacancy induces a uniform magnetic moment in the ground state [65]. As a result, a
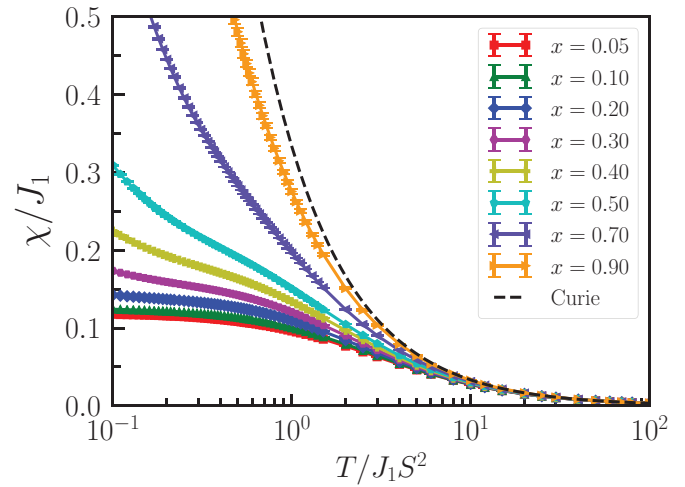

FIG. 8. Simulation results for the magnetic susceptibility per spin $\chi(T)/N_s$ of the classical Heisenberg model in Eq. (3) with $J_2/J_1 = 0.12$ for different concentrations x of magnetic vacancies. The simulations were performed for $L = 30$; finite-sized effects are minimal for the temperatures shown.

weak residual Curie term in the susceptibility at very low T is expected even for small nonzero x [65,66]. For a model with nearest-neighbor coupling only, the threshold for site percolation is $x_p = \frac{1}{2}$, such that a system with statistically distributed vacancies and $x > x_p$ consists of magnetically disconnected finite-sized clusters only. Consequently, larger Curie contributions (per spin) are expected, arising from clusters with an odd number of sites, which grow as $x \rightarrow 1$. Small nonzero values of J_2 will produce only small corrections to this picture.

Simulation results for the normalized linear-response magnetic susceptibility $\chi(T)/N_s$ are shown in Fig. 8 for different levels of dilution. While $\chi(T)$ follows a CW law for all x at elevated T, it tends to saturate upon cooling for small x in the T range shown but strongly increases for large x. The $x = 0.9$ result is not far from a pure Curie law, consistent with the above considerations.

The CW law can be analyzed quantitatively: High-temperature expansion for the diluted Heisenberg antiferromagnet yields the exact result [67] $k_B|\theta| = (1 - x)S(S + 1)z(J_1 + J_2)/3$, with $z = 6$ being the number of nearest-neighbor sites. This qualitative x dependence $\theta(x) = (1 - x)\theta(x=0)$ is in good agreement with the ESR-extracted linearity in Fig. 6 (right frame). From matching the CW temperature at $x = 0$, $\theta(x=0) = 11.2$ K (taken from magnetic susceptibility), we can extract a nearest-neighbor coupling of $J_1 = 7.5$ K if we assume $J_2 = 0$, or $J_1 = 6.7$ K for $J_2/J_1 = 0.12$, the former in agreement with Ref. [13].

For a quantitative comparison between the simulation and experiment of the full temperature dependence of χ, we need to consider that the natural energy scale for the classical magnet is J_1S^2, while this is replaced for the quantum magnet by $J_1S(S + 1)$. The plot of the susceptibility data with the data from the simulation shows fairly good agreement (Fig. S12 in the Supplemental Material [44]). The best match was found for $(J_1S^2)_{cl} = 4$ K, corresponding to an exchange coupling J_1 of ~ 5.3 K, but some deviations between calculation and experiment remain at low temperatures, particularly for doped

samples. They may originate in additional contributions to the experimental susceptibility, either intrinsic (van Vleck) or extrinsic (background signal of the sample holder), but they may also reflect the fact that the J_1-J_2 Heisenberg model is not sufficient to fully capture the physics of the material which in fact can be expected to display significant spin-orbit coupling.

IV. CONCLUSIONS

The solid-solution series $NaYb_{1-x}Lu_xS_2$ was established for $0 \leqslant x \leqslant 1$, where Yb and Lu occupy the B site of the $3R$ α-NaFeO$_2$ structure statistically. The lattice parameters of the series ideally follow Vegard's rule, and neither evidence for a phase segregation nor for an ordered superstructure was found. The bandgaps change only for high Lu contents, and the magnetic susceptibility reflects the amount of Yb^{3+} ions. The ESR spectra of $NaYb_{1-x}Lu_xS_2$ show clear dependencies on the Yb^{3+} content. It was shown that small differences in the lattice parameters upon changing the Yb^{3+} amount produce small changes in the crystal fields and the g values of the effective spin-$\frac{1}{2}$ Kramers Yb^{3+} doublets. Also, the interaction among the Yb^{3+} spins, as reflected in the ESR linewidth and ESR intensity, as well as in Weiss temperatures, changes with Yb^{3+} amount. The line shape for the lowest investigated Yb amount of $x = 0.9$ has clear features typical for a hyperfine splitting, indicating single-ion behavior of independent Yb^{3+} spins.

In summary, we have shown that the magnetic exchange network of NaYbS$_2$ can be tuned by a random Lu substitution on the Yb site while maintaining the strong frustration. Further measurements, such as heat capacity, AC susceptibility, or μSR spectroscopy, in the sub-Kelvin regime are necessary and scheduled to examine if the QSL state is preserved upon Lu doping up to the percolation threshold, as suggested by our present results. Thus, nonmagnetic substitution opens up a direction in QSL research, e.g., to elucidate to what extent the magnetic field–temperature phase diagram is affected by the controlled dilution.

[1] P. W. Anderson, Mater. Res. Bull. **8**, 153 (1973).

[2] J. Knolle and R. Moessner, Annu. Rev. Condens. Matter Phys. **10**, 451 (2019).

[3] A. Banerjee, C. A. Bridges, J.-Q. Yan, A. A. Aczel, L. Li, M. B. Stone, G. E. Granroth, M. D. Lumsden, Y. Yiu, J. Knolle, S. Bhattacharjee, D. L. Kovrizhin, R. Moessner, D. A. Tennant, D. G. Mandrus, and S. E. Nagler, Nat. Mater. **15**, 733 (2016).

[4] Y. Singh and P. Gegenwart, Phys. Rev. B **82**, 064412 (2010).

[5] Y. Li, G. Chen, W. Tong, L. Pi, J. Liu, Z. Yang, X. Wang, and Q. Zhang, Phys. Rev. Lett. **115**, 167203 (2015).

[6] Z. Zhu, P. A. Maksimov, S. R. White, and A. L. Chernyshev, Phys. Rev. Lett. **119**, 157201 (2017).

[7] K. Kitagawa, T. Takayama, Y. Matsumoto, A. Kato, R. Takano, T. Kishimoto, S. Bette, R. Dinnebier, G. Jackeli, and H. Takagi, Nature (London) **554**, 341 (2018).

[8] M. Baenitz, P. Schlender, J. Sichelschmidt, Y. A. Onykiienko, Z. Zangeneh, K. M. Ranjith, R. Sarkar, L. Hozoi, H. C. Walker, J.-C. Orain, H. Yasuoka, J. van den Brink, H.-H. Klauss, D. S. Inosov, and T. Doert, Phys. Rev. B **98**, 220409(R) (2018).

[9] W. Liu, Z. Zhang, J. Ji, Y. Liu, J. Li, X. Wang, H. Lei, G. Chen, and Q. Zhang, Chin. Phys. Lett. **35**, 117501 (2018).

[10] K. M. Ranjith, D. Dmytriieva, S. Khim, J. Sichelschmidt, S. Luther, D. Ehlers, H. Yasuoka, J. Wosnitza, A. A. Tsirlin, H. Kühne, and M. Baenitz, Phys. Rev. B **99**, 180401(R) (2019).

[11] M. M. Bordelon, E. Kenney, C. Liu, T. Hogan, L. Posthuma, M. Kavand, Y. Lyu, M. Sherwin, N. P. Butch, C. Brown, M. J. Graf, L. Balents, and S. D. Wilson, Nat. Phys. **15**, 1058 (2019).

[12] K. M. Ranjith, S. Luther, T. Reimann, B. Schmidt, P. Schlender, J. Sichelschmidt, H. Yasuoka, A. M. Strydom, Y. Skourski,

J. Wosnitza, H. Kühne, T. Doert, and M. Baenitz, Phys. Rev. B **100**, 224417 (2019).

[13] B. Schmidt, J. Sichelschmidt, K. M. Ranjith, T. Doert, and M. Baenitz, Phys. Rev. B **103**, 214445 (2021).

[14] R. D. Shannon, D. B. Rogers, and C. T. Prewitt, Inorg. Chem. **10**, 713 (1971).

[15] J. Xing, L. D. Sanjeewa, J. Kim, G. R. Stewart, A. Podlesnyak, and A. S. Sefat, Phys. Rev. B **100**, 220407(R) (2019).

[16] H. A. Ceccatto, C. J. Gazza, and A. E. Trumper, Phys. Rev. B **47**, 12329(R) (1993).

[17] R. Kaneko, S. Morita, and M. Imada, J. Phys. Soc. Jpn. **83**, 093707 (2014).

[18] Z. Zhu and S. R. White, Phys. Rev. B **92**, 041105(R) (2015).

[19] Y. Iqbal, W.-J. Hu, R. Thomale, D. Poilblanc, and F. Becca, Phys. Rev. B **93**, 144411 (2016).

[20] Z. Zhu, P. A. Maksimov, S. R. White, and A. L. Chernyshev, Phys. Rev. Lett. **120**, 207203 (2018).

[21] P. A. Maksimov, Z. Zhu, S. R. White, and A. L. Chernyshev, Phys. Rev. X **9**, 021017 (2019).

[22] D. S. Rokhsar and S. A. Kivelson, Phys. Rev. Lett. **61**, 2376 (1988).

[23] C. Peng, Y.-F. Jiang, D.-N. Sheng, and H.-C. Jiang, Adv. Quantum Technol. **4**, 2000126 (2021).

[24] N. Nagaosa, A. Furusaki, M. Sigrist, and F. H., J. Phys. Soc. Jpn. **65**, 3724 (1996).

[25] F. Zschocke and M. Vojta, Phys. Rev. B **92**, 014403 (2015).

[26] T. Bilitewski, M. E. Zhitomirsky, and R. Moessner, Phys. Rev. Lett. **119**, 247201 (2017).

[27] J. Knolle, R. Moessner, and N. B. Perkins, Phys. Rev. Lett. **122**, 047202 (2019).

[28] S. Sachdev and M. Vojta, in *Proceedings of the XIII International Congress on Mathematical Physics*, edited by A. Fokas, A. Grigoryan, T. Kibble, and B. Zegarlinski (International Press, London, 2001)

[29] E. C. Andrade and M. Vojta, Europhys. Lett. **97**, 37007 (2012).

[30] M. Fujisawa, T. Ono, H. Fujiwara, H. Tanaka, V. Sikolenko, M. Meissner, P. Smeibidl, S. Gerischer, and H. A. Graf, J. Phys. Soc. Jpn. **75**, 033702 (2006).

[31] S. Dommange, M. Mambrini, B. Normand, and F. Mila, Phys. Rev. B **68**, 224416 (2003).

[32] A. Sen and R. Moessner, Phys. Rev. Lett. **114**, 247207 (2015).

[33] A. J. Willans, J. T. Chalker, and R. Moessner, Phys. Rev. Lett. **104**, 237203 (2010).

[34] G. J. Sreejith, S. Bhattacharjee, and R. Moessner, Phys. Rev. B **93**, 064433 (2016).

[35] K. Watanabe, H. Kawamura, H. Nakano, and T. Sakai, J. Phys. Soc. Jpn. **83**, 034714 (2014).

[36] Y. Li, D. Adroja, R. I. Bewley, D. Voneshen, A. A. Tsirlin, P. Gegenwart, and Q. Zhang, Phys. Rev. Lett. **118**, 107202 (2017).

[37] H. Yamaguchi, M. Okada, Y. Kono, S. Kittaka, T. Sakakibara, T. Okabe, Y. Iwasaki, and Y. Hosokoshi, Sci. Rep. **7**, 16144 (2017).

[38] H.-Q. Wu, S.-S. Gong, and D. N. Sheng, Phys. Rev. B **99**, 085141 (2019).

[39] S. Kundu, A. Hossain, S. Pranava Keerthi, R. Das, M. Baenitz, P. J. Baker, J.-C. Orain, D. C. Joshi, R. Mathieu, P. Mahadevan, S. Pujari, S. Bhattacharjee, A. V. Mahajan, and D. D. Sarma, Phys. Rev. Lett. **125**, 117206 (2020).

[40] Z.-X. Luo, E. Lake, J.-W. Mei, and O. A. Starykh, Phys. Rev. Lett. **120**, 037204 (2018).

[41] B. Miksch, A. Pustogow, M. J. Rahim, A. A. Bardin, K. Kanoda, J. A. Schlueter, R. Hübner, M. Scheffler, and M. Dressel, Science **372**, 276 (2021).

[42] J. Sichelschmidt, P. Schlender, B. Schmidt, M. Baenitz, and T. Doert, J. Phys.: Condens. Matter **31**, 205601 (2019).

[43] H. Masuda, T. Fujino, N. Sato, and K. Yamada, Mater. Res. Bull. **34**, 1291 (1999).

[44] See Supplemental Material at http://link.aps.org/supplemental/10.1103/PhysRevMaterials.6.046201 for details of sample preparation and additional crystallographic, ESR, and magnetization data.

[45] A. A. Coelho, J. Appl. Crystallogr. **51**, 210 (2018).

[46] A. W. Verheijen, W. J. P. V. Enckevort, J. Bloem, and L. J. Giling, J. Phys. Colloques **36**, C3 (1975).

[47] G. M. Sheldrick, Acta Crystallogr. C Struct. Chem. **71**, 3 (2015).

[48] O. V. Dolomanov, L. J. Bourhis, R. J. Gildea, J. A. K. Howard, and H. Puschmann, J. Appl. Crystallogr. **42**, 339 (2009).

[49] P. Kubelka and F. Munk, Z. Tech. Phys. **12**, 593 (1931).

[50] J. Tauc, R. Grigorovici, and A. Vancu, Phys. Status Solidi B **15**, 627 (1966).

[51] S. Campbell, I. Herbert, C. Warwick, and J. Woodgate, J. Phys. E **9**, 443 (1976).

[52] V. Jarý, L. Havlák, J. Bárta, M. Buryi, E. Mihóková, M. Rejman, V. Laguta, and M. Nikl, Materials **8**, 6978 (2015).

[53] B. Deng, D. E. Ellis, and J. A. Ibers, Inorg. Chem. **41**, 5716 (2002).

[54] L. Havlák, V. Jarý, M. Nikl, P. Boháček, and J. Bárta, Acta Mater. **59**, 6219 (2011).

[55] R. D. Shannon, Acta Crystallogr. Sect. A **32**, 751 (1976).

[56] T. Gambke, B. Elschner, R. Kremer, and M. Schanz, J. Magn. Magn. Mater. **36**, 115 (1983).

[57] S. K. Misraand S. Isber, Phys. B: Condens. Matter **253**, 111 (1998).

[58] J. Sichelschmidt, B. Schmidt, P. Schlender, S. Khim, T. Doert, and M. Baenitz, JPS Conf. Proc. **30**, 011096 (2020).

[59] A. Abragam and B. Bleaney, *Electron Paramagnetic Resonance of Transition Ions* (Oxford University Press, Oxford, 1970).

[60] J. P. Wolfe and C. D. Jeffries, Phys. Rev. B **4**, 731 (1971).

[61] T. Gruner, J. Wykhoff, J. Sichelschmidt, C. Krellner, C. Geibel, and F. Steglich, J. Phys.: Condens. Matter **22**, 135602 (2010).

[62] U. Arjun, K. M. Ranjith, B. Koo, J. Sichelschmidt, Y. Skourski, M. Baenitz, A. A. Tsirlin, and R. Nath, Phys. Rev. B **99**, 014421 (2019).

[63] M. Baenitz, M. M. Piva, S. Luther, J. Sichelschmidt, K. M. Ranjith, H. Dawczak-Dębicki, M. O. Ajeesh, S.-J. Kim, G. Siemann, C. Bigi, P. Manuel, D. Khalyavin, D. A. Sokolov, P. Mokhtari, H. Zhang, H. Yasuoka, P. D. C. King, G. Vinai, V. Polewczyk, P. Torelli *et al.*, Phys. Rev. B **104**, 134410 (2021).

[64] A. V. Chubukov and T. Jolicoeur, Phys. Rev. B **46**, 11137 (1992).

[65] A. Wollny, L. Fritz, and M. Vojta, Phys. Rev. Lett. **107**, 137204 (2011).

[66] V. S. Maryasin and M. E. Zhitomirsky, J. Phys.: Conf. Ser. **592**, 012112 (2015).

[67] K. Binder and A. P. Young, Rev. Mod. Phys. **58**, 801 (1986).